Applied Energy 253 (2019) 113608

Contents lists available at ScienceDirect

Applied Energy

journal homepage: www.elsevier.com/locate/apenergy

Optimization of the self-condensing CO_2 transcritical power cycle using solar thermal energy

Lisheng Pan[a,*], Bing Li[b], Weixiu Shi[b], Xiaolin Wei[a,c]

[a] State Key Laboratory of High-temperature Gas Dynamics, Institute of Mechanics, Chinese Academy of Sciences, Beijing 100190, China
[b] School of Environment and Energy Engineering, Beijing University of Civil Engineering and Architecture, Beijing 100044, China
[c] School of Engineering Sciences, University of Chinese Academy of Sciences, Beijing 100049, China

HIGHLIGHTS

- The novel CO_2 transcritical power cycle operates with conventional water cooling.
- Theoretical study was executed on the relationships among the cycle's parameters.
- The novel cycle simplifies the development of the pressurizing component.

GRAPHICAL ABSTRACT

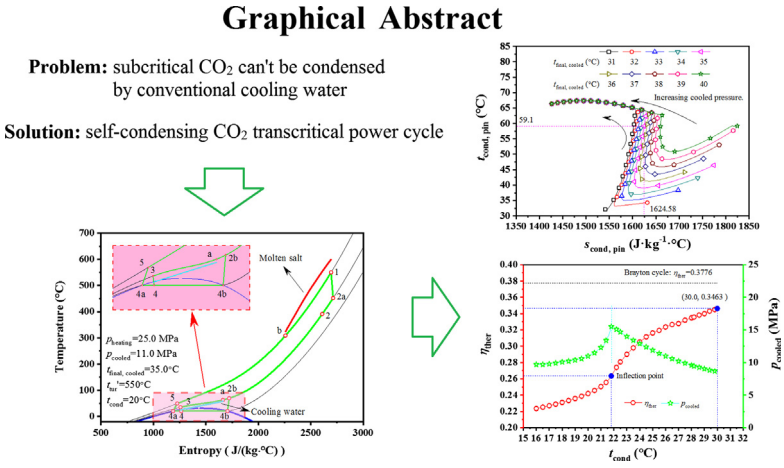

ARTICLE INFO

Keywords:
CO_2 transcritical power cycle
Supercritical CO_2 Brayton cycle
Solar thermal energy
CO_2 condensation

ABSTRACT

Compared with the conventional Rankine cycle, the CO_2 transcritical power cycle gives a higher thermal efficiency because of its high average heat absorbing temperature and is suitable for driving a compact system. The self-condensing CO_2 transcritical power cycle can solve the problem that CO_2 is difficult to condense in a conventional CO_2 transcritical power cycle using conventional water cooling. Based on solar thermal energy, a theoretical analysis model was established to study the relationship between the cycle performance and the operating parameters. The results showed that the thermal efficiency increases with increasing the cooled pressure with a low final cooled temperature. By increasing the final cooled temperature, a peak appears on the thermal efficiency curve. The outlet temperature of the cooling water is affected by a shift of the pinch point position in the cooler. According to the variation of the outlet temperature of the cooling water and the proportion of the mass flow rate of CO_2 in the power sub-cycle and that in the whole cycle, it can be concluded that conditions with a very low cooled pressure are uncontrollable. In these conditions, the maximum thermal efficiency of the self-condensing CO_2 transcritical cycle is 0.3463, which is 0.0313 a little lower than that of the supercritical CO_2 Brayton cycle. However, the novel cycle simplifies the development of the pressurizing component and avoids the liquid hammer in the pressurizing process.

* Corresponding author.
E-mail address: panlisheng@imech.ac.cn (L. Pan).

https://doi.org/10.1016/j.apenergy.2019.113608
Received 26 February 2019; Received in revised form 17 July 2019; Accepted 21 July 2019
Available online 31 July 2019

Nomenclature

t	temperature (°C)
p	pressure (MPa)
C	specific heat capacity ($J{\cdot}kg^{-1}{\cdot}°C^{-1}$)
s	entropy ($J{\cdot}kg^{-1}{\cdot}°C^{-1}$)
$\dot{P}$	power (kW)
$\dot{Q}$	heat capacity (kW)
η	efficiency
$\dot{m}$	mass flow rate of the working fluid ($kg{\cdot}s^{-1}$)

subscript

p	isobaric
b	boiling
c	critical
pum	pump
exp	expander
com	compressor
ther	thermal
pin	pinch point
cond	condensing
1, 2, 2a, 2b, 3, 4, 4a, 4b, 5, a, b	state points of the transcritical power cycle

superscript

′	inlet
″	outlet

1. Introduction

A working fluid with low boiling temperature gives better performance than water in power cycles, especially in using low temperature heat source [1]. CO_2 is an important unconventional working which is attracting more and more attention [2]. It can operates efficiently using not only a low temperature heat source but also a high temperature heat source. For high temperature heat source, it can provide much higher thermal efficiency than water because of its high average heat absorbing temperature, but a large regenerator should be used to recover the heat of CO_2 exhaust from the turbine. In high thermal efficiency conditions, a basic CO_2 power cycle can't cool the exhaust gas to a sufficiently low temperature (e.g. 200 °C) using fossil energy sources. Therefore, it is more suitable for converting solar thermal energy and nuclear energy which usually integrate with a circulation system of a heat transfer medium. Solar thermal energy is an important renewable and clean energy source that has already attracted considerable attention. It is very important to exploit and utilize solar thermal energy effectively as a supplement of fossil energy [3].

CO_2 also has some good thermal properties, such as high thermal stability and in addition a low Global Warming Potential (GWP), a zero Ozone Depletion Potential (ODP). It is further nontoxic and nonflammable [4], which indicates that this natural substance has less influence than the Freon on the environment. Because the supercritical CO_2 has a much lower viscosity, compact heat exchangers can be used for the supercritical heater, the condenser, the cooler, and especially the regenerator. A compact radial inflow turbine can also be used for the expansion of the supercritical CO_2. Therefore, the CO_2 power cycle usually has a smaller size than the Rankine cycle. Because of its cheapness, the operating cost is much lower than the other unconventional working fluids.

According to a theoretical analysis, Ding et al. [5] pointed out that a CO_2 transcritical power cycle gives higher thermal efficiency than a power cycle using organic fluids such as R22, R600, R123, R134a or R12. Zhang et al. studied the cycle efficiency of a CO_2 transcritical power cycle with their experimental system using a throttle valve instead of an expander or a turbine [6] and tested an experimental hydrogen production system using a CO_2 cycle based on solar energy [7]. Pan et al. [8] established a CO_2 transcritical power cycle and obtained 1.1 kW of a stable electric power. This cycle was also used to recover waste heat from engine exhaust [9]. Kim et al. [10] compared a CO_2 transcritical power cycle and a supercritical CO_2 power cycle using low temperature heat and high temperature heat sources, respectively. Wang et al. [11] compared different cycle layouts of supercritical CO_2 Brayton cycles integrated with molten salt solar power towers. Minh et al. [12] investigated the operation of supercritical CO_2 Brayton cycles in transient conditions. Chacartegui et al. [13] integrated a CO_2 power cycle with thermochemical energy storage of a concentrated solar power. Xu et al. [14] improved the supercritical coal-fired power generation system by incorporating a supplementary supercritical CO_2 cycle. Olumayegun et al. [15] also considered CO_2 capture in the coal-fired power generation system with a supercritical CO_2 closed Brayton cycle. Moullec [16] carried out the conceptual study of a high efficiency coal-fired power plant with CO_2 Brayton cycle. Sun et al. [17] carried out exergy analysis and optimization of a hydrogen production process with a solar-liquefied natural gas hybrid driven transcritical CO_2 power cycle in which liquefied natural gas can provide sufficiently low temperature to condense CO_2. Exergetic analysis was also carried out by Padilla et al. on the supercritical CO_2 Brayton cycle integrated with solar central receivers [18]. Zhao et al. [19] used liquid natural gas as a cold source to drive a hybrid system integrated with compressed air energy storage and a CO_2 transcritical power cycle. Padilla et al. [20] proposed three supercritical CO_2 Brayton cycle configurations assisted by an ejector and pointed out that the recompression with an ejector and intercooling gives the best thermal efficiency. Syblik et al. [21] analysed the cycle performance of two supercritical CO_2 Brayton power cycles that are used to cool the specific fusion reactor.

However, it is difficult to condense the subcritical CO_2 with conventional water cooling in a conventional CO_2 transcritical power cycle because of the low critical temperature. This disadvantage seriously limits the actual application of a CO_2 transcritical power cycle. Pan et al. [22] pointed out that a transcritical power cycle using a CO_2-based mixture can solve the condensing problem by raising the critical temperature. Zeotropic mixtures attracted a lot of attention in the field of organic Rankine cycle [23]. Xia et al. [24] also studied the thermodynamic and thermo-economic performance of a transcritical power cycle using CO_2-based mixture as working fluid. Nevertheless, the low thermal stability of the mixture limits this type cycle to low temperature heat source because most of the considered second components are organics that are decomposed easier than CO_2. Dai et al. carried out an experimental study on thermal stability of some hydrocarbons [25] and hydrofluorocarbons [26] for a transcritical power cycle. In addition, the combustion characteristic of the CO_2-based mixtures should be paid attention to besides the cycle performance [27]. Pan et al. [28] proposed a novel CO_2 transcritical power cycle, namely, a self-condensing CO_2 transcritical power cycle, to avoid the cooling problem and analysed it with low temperature heat source using a theoretical approach. The cooling problem is solved completely in the above two transcritical power cycles. The self-condensing CO_2 transcritical power cycle can be used not only for low temperature heat sources but also for high

temperature heat sources.

There is still a lack of the research on self-condensing CO_2 transcritical power, especially about the relationship among the cycle's parameters and the optimization method for this novel cycle. Therefore, a theoretical analysis model for the self-condensing CO_2 transcritical power cycle was established, and a detailed investigation was executed with the aim to reveal the relationships between the cycle performance and the operating parameters. As one of the most potential application areas, solar thermal energy was used to drive the cycle with molten salt as heat transfer medium.

2. Methodology

2.1. System and modelling

As shown in Fig. 1, the main components of a self-condensing CO_2 transcritical power cycle system include a heater, a turbine, a cooler, an expander, a vapour-liquid separator, a compressor, a pump and a regenerator. For a CO_2 power cycle, a large regenerator is necessary because of the high temperature of CO_2 exhausted from the turbine. In the supercritical heater, supercritical CO_2 is heated from state b to state 1. An expansion occurs in the turbine with outputting shaft power simultaneously. Two CO_2 flows (state 2a and state 2b) mix together (state 2). Next, all of the CO_2 enters the regenerator and is cooled to state a. The cooling water is used to cool the supercritical CO_2 even further in the cooler. The cool supercritical CO_2 at state 3 enters the expander and expands to state 4. In the vapour-liquid separator, the saturated liquid (4a) and the saturated vapour (4b) separate from the two-phase CO_2 flow. The vapour is compressed from state 4b to state 2b, while the saturated liquid is pressurized by a pump from state 4a to state 5. Then, the cold liquid CO_2 under the supercritical pressure enters the regenerator to absorb the remaining heat from the exhaust CO_2. Solar thermal energy is used to raise the temperature of the supercritical CO_2 further from state b to state 1.

The whole cycle consists of two sub-cycles, namely, the power sub-cycle (4-4a-5-b-1-2a-2-3-4) and refrigeration sub-cycle (4-4b-2b-2-a-3-4). The power sub-cycle is the main cycle in which the turbine outputs shaft power and the pump consumes some of it. The refrigeration sub-cycle is an auxiliary cycle which provides liquid CO_2 for the power sub-cycle. Much shaft power can also be recovered by the expander, while the compressor consumes more power than recovered.

It is worth noting that the expander operates in the two-phase region where is harmful to an impeller. In fact, the density difference between liquid and vapour is much less near the critical point than that in the other two-phase regions. This may decrease the impact of liquid hammer on the impeller. However, non-impeller expander should be used for safer operation, such as a piston expander, a screw expander and so on. Furthermore, the expander can also be replaced by a throttle valve. Using this method, the issue about the liquid hammer on the expander can be avoided, but the expansion power is lost.

2.2. Calculation process

The theoretical calculation process is indicated in Fig. 2. The thermophysical properties of CO_2 at all states are obtained from REFPROP 9.0 [29] by inputting some of the state parameters.

In the turbine and the expander, the temperature and the pressure of CO_2 decrease during the expansion process, as well as the specific enthalpy. The turbine inlet state can be specified by the heated pressure and the inlet temperature. For the expander, it can be determined by the cooled pressure and the final cooled temperature. Consequently, with the inlet parameters and the isentropic efficiency, the enthalpy at the exit of the turbine and the expander can be calculated according to Eq. (1). Here, the definition and the naming method, should be noted, for some parameters such as the heated pressure, the final cooled temperature, the cooled pressure and the final cooled temperature. The heated pressure refers the pressure under which the CO_2 is heated in the supercritical heater and the final heated temperature represents the temperature of the supercritical CO_2 at the exit of the heater. Similarly, the working fluid, CO_2, is cooled to the 'final cooled temperature' by the cooling water under the 'cooled pressure'.

$$\eta_{\text{isen,tur}} = \frac{h_1 - h_{2a}}{h_1 - h_{2a,\text{isen}}} \tag{1a}$$

$$\eta_{\text{isen,exp}} = \frac{h_3 - h_4}{h_3 - h_{4,\text{isen}}} \tag{1b}$$

The CO_2 from the turbine and the CO_2 from the compressor mixes together and flows forward to the regenerator to heat the cold working fluid from the pump. It is worth noting that the mass flow rate of the hot CO_2 is higher than that of the cold CO_2. Therefore, the heat balance equation can be expressed as,

$$\dot{m}_{\text{total}}\cdot(h_2 - h_a) = \dot{m}_{\text{power}}\cdot(h_b - h_5) \tag{2}$$

In the cooler, the heat capacity is expressed as Eq. (3a) and the state of CO_2 at the exit of the cooler is determined by the cooled pressure and the final cooled temperature. Under specified cycle, the outlet temperature of the cooling water is determined by the pinch point temperature difference in the cooler. Then, the mass flow rate of the cooling water can be found with Eq. (3b).

$$\dot{Q}_{\text{cond}} = \dot{m}_{\text{total}}\cdot(h_a - h_3) \tag{3a}$$

$$\dot{Q}_{\text{cond}} = \dot{m}_{\text{cooling}}\cdot(t''_{\text{cooling}} - t'_{\text{cooling}}) \tag{3b}$$

With the known inlet parameters and isentropic efficiency, the outlet parameters of the pump and the compressor can be calculated according to Eq. (4).

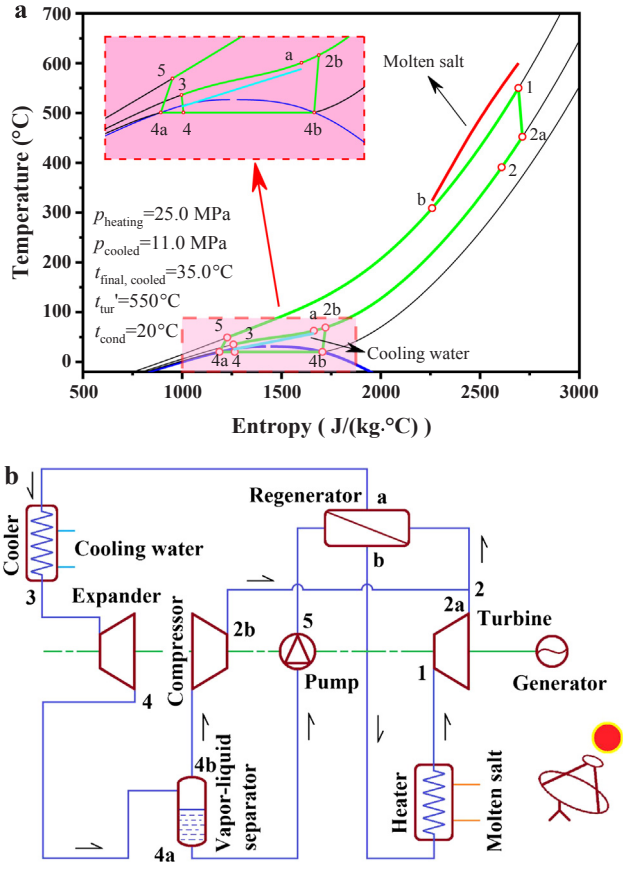

Fig. 1. Schematic diagram and flow chart of the self-condensing CO_2 transcritical power cycle. (a Schematic diagram; b Flow chart).

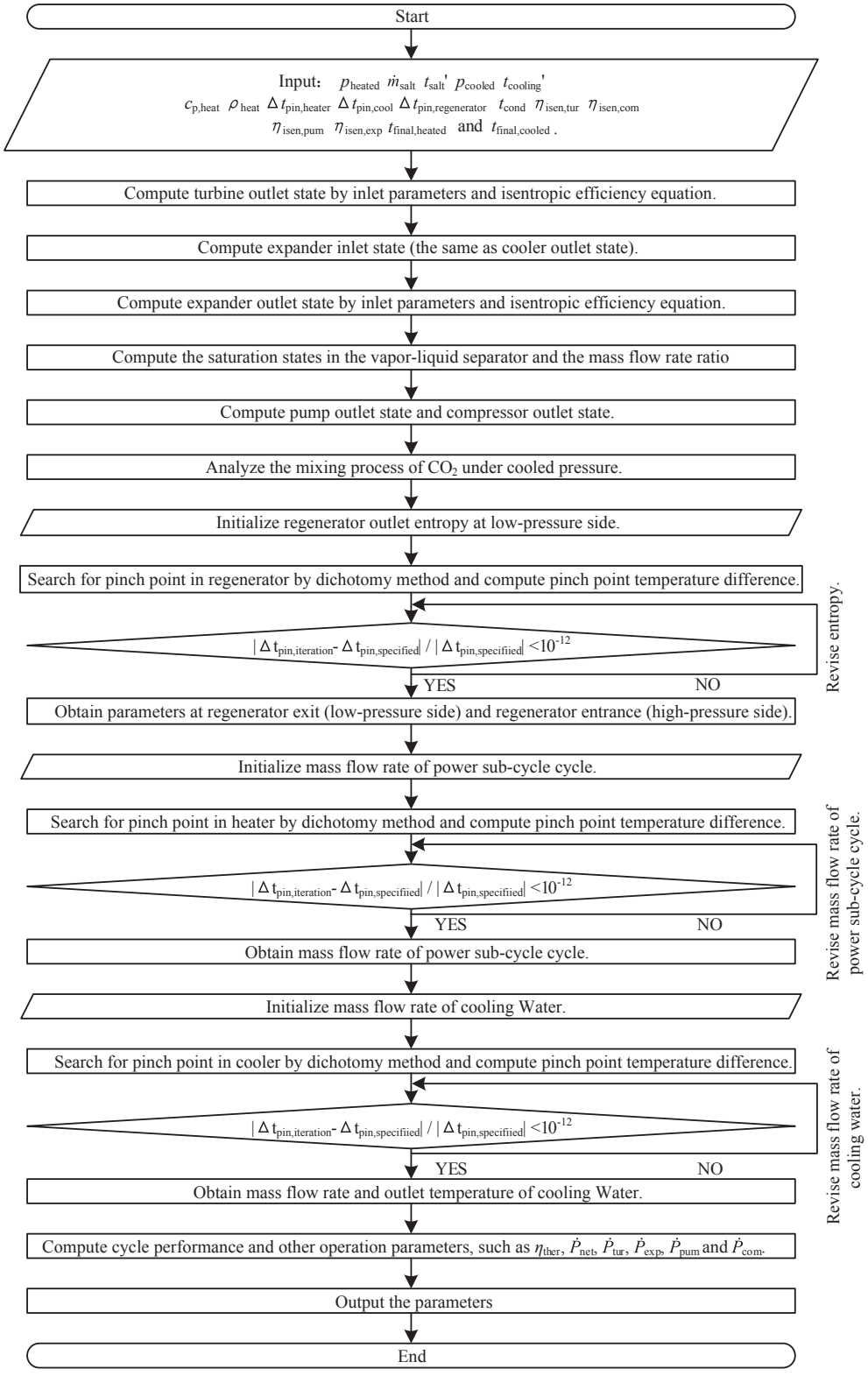

Fig. 2. Flow chart of the calculation process.

$$\eta_{\text{isen,pump}} = \frac{h_{5,\text{isen}} - h_{4a}}{h_5 - h_{4a}} \tag{4a}$$

$$\eta_{\text{isen,compressor}} = \frac{h_{2b,\text{isen}} - h_{4b}}{h_{2b} - h_{4b}} \tag{4b}$$

The heat capacity in the supercritical heater can be expressed as Eq. (5). The mass flow rate of CO_2 in the power sub-cycle and the heater outlet temperature are used to ensure that the pinch point temperature difference in the supercritical heater is equal to the specified value.

$$\dot{Q}_{\text{heater}} = \dot{m}_{\text{power}} \cdot (h_1 - h_b) \tag{5a}$$

$$\dot{Q}_{\text{heater}} = \dot{m}_{\text{salt}} \cdot (t'_{\text{salt}} - t''_{\text{sat}}) \tag{5b}$$

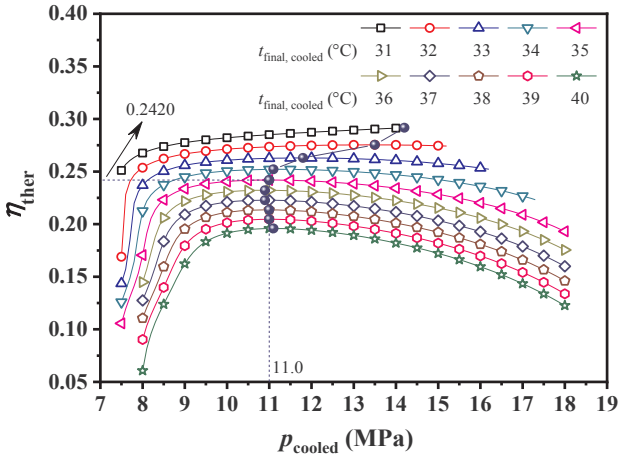

Fig. 3. Variation in the thermal efficiency with cooled pressure under different final cooled temperatures.

2.3. Performance indicator

The net output power and the thermal efficiency are the most important performance indicators. In a self-condensing CO_2 transcritical power cycle, the turbine and the expander generate power, while the pump and the compressor consume power. Therefore, the net output power can be expressed as

$$\dot{P}_{net} = (\dot{P}_{tur} - \dot{P}_{pum}) - (\dot{P}_{com} - \dot{P}_{exp}) \tag{6}$$

Heat is absorbed by supercritical CO_2 in the supercritical heater and the thermal efficiency can be represented as a ratio of the net output power to the heat capacity of the supercritical heater, as shown in Eq. (7).

$$\eta_{ther} = \frac{\dot{P}_{net}}{\dot{Q}_{heater}} \tag{7}$$

The temperature and the pressure of the supercritical CO_2 at the exit of the cooler dominate the state of point 3 which impacts the mass flow rate and the performance of each sub-cycle. For example, under a constant pressure, a low outlet temperature of the cooler is helpful for increasing the mass flow rate in the power sub-cycle and improving the whole cycle performance. The refrigeration sub-cycle is an auxiliary cycle that generates cooling capacity to condense CO_2 for the pump in the power sub-cycle. Therefore, these two parameters specified as the final cooled temperature and the cooled pressure are very important and should be optimized and controlled in practical systems to improve the whole cycle performance. It is worth noting that the condensing temperature also affects the cycle performance.

2.4. Data source

Molten salt is a common heat transfer medium that is usually used in solar thermal energy systems. The temperature range for application is usually determined by its thermophysical properties. In the following analysis, the considered temperature range is from 60 °C to 600 °C. It is difficult to find a suitable medium that can be used in such a wide range. Therefore, the extrapolation method is used to calculate the specific heat capacity if the temperature exceeds the limited range. Though this method influences the outlet temperature and the mass flow rate of the molten salt a little, it does not affect the cycle performance and the operating parameters.

Eqs. (8) and (9) are used to calculate the density and the specific heat capacity of the molten salt, respectively [30]. An extrapolation method is used to calculate the specific heat capacity when the temperature is lower than 286.9 °C.

$$\rho = 2430.2 - 0.4347t \tag{8}$$

$$C_p = 347.08 + 2.6t \quad [286.9 - 430.3\ °C] \tag{9a}$$

$$C_p = -3324.59 + 7.8t \quad [430.3 - 746.9\ °C] \tag{9b}$$

In the theoretical analysis, the following parameters are specified. The mass flow rate of the molten salt is specified as 10 $kg{\cdot}s^{-1}$. The inlet temperature of the molten salt is 600 °C. The supercritical heated pressure is 25.0 MPa. Temperature at the turbine entrance is 550 °C. The isentropic efficiency of the pump, turbine, compressor and expander are specified as 0.65, 0.88, 0.80 and 0.75, respectively. The pinch point temperature differences in the cooler and the regenerator are specified as 5 °C and 10 °C, respectively. Because of the poor heat transfer of the molten salt, the pinch point temperature difference in the supercritical heater is specified as 15 °C. The inlet temperature of the cooling water is 25 °C. The final cooled temperature range is from 31 °C to 40 °C while the cooled pressure range is from 7.5 MPa to 18.0 MPa.

3. Results and discussion

In this section, several performance indicators and operating parameters are studied using the above theoretical approach. The cooled pressure and condensing temperature are optimized to enhance the thermal efficiency.

3.1. Optimization of the cooled pressure

During the optimization of the cooled pressure, a constant condensing temperature is specified as 20 °C.

As shown in Fig. 3, thermal efficiency increases with increasing the cooled pressure with a final cooled temperature of 31 °C. When the final cooled temperature is in the range from 32 °C to 40 °C, the thermal efficiency curve has a peak. With a constant final cooled temperature, the higher the cooled pressure is, the more the saturated liquid is in the vapour-liquid separator. More saturated liquid or higher mass flow rate in the power sub-cycle power cycle contribute to the thermal efficiency of the whole cycle. However, it is harmful to the enhancement of the turbine output power to increase the cooled pressure, because it also reduces the specific enthalpy drop in the turbine. With a final cooled temperature range from 32 °C to 40 °C, the effect of the turbine power output on the thermal efficiency is more obvious than the mass flow rate when the cooled pressure reaches a certain value. Therefore, a peak appears on the thermal efficiency curve.

As shown in Fig. 4, with a constant cooled pressure the proportion of the saturated liquid in the vapour-liquid separator decreases with

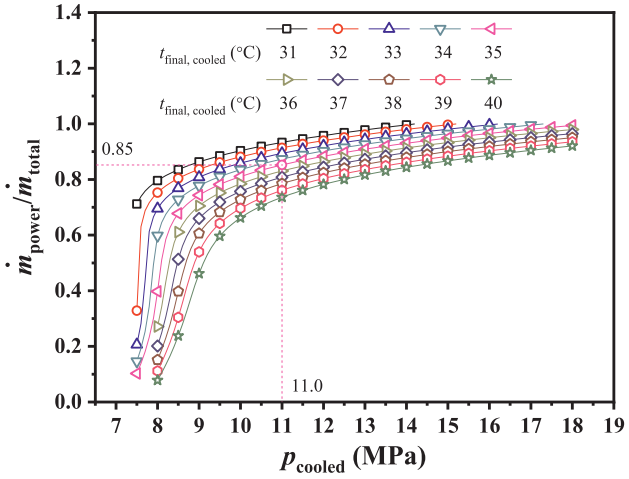

Fig. 4. The proportion between mass flow rate of CO_2 in the power sub-cycle and that in the whole cycle.

increasing the final cooled temperature, which causes a negative correlation between thermal efficiency and cooled temperature.

Under a low final cooled temperature, such as 31 °C, the proportion of saturated liquid in the vapour-liquid separator can reach 1.0 with a high enough cooled pressure. In other words, the cooled supercritical CO_2 expands to a bubble point or supercooled region and no vapour separates from the vapour-liquid separator. Without the vapour separating these conditions become meaningless for this novel power cycle and are omitted in the analysis. Though the maximum efficiency appears under 14.2 MPa with a final cooled temperature of 31 °C in the considered conditions, it is still difficult to cool supercritical CO_2 to near 31 °C using conventional water cooling. On the other hand, because CO_2 has a critical temperature of approximately 31 °C, its thermophysical properties are very sensitive to the operating parameters, such as temperature and pressure. Therefore, 35 °C is selected as the optimal final cooled temperature. Consequently, the maximum thermal efficiency is 0.2420 with a cooled pressure of 11.0 MPa in these considered conditions. It is also noted that the optimal cooled pressure decreases obviously and then keeps nearly constant at 11.0 MPa with increasing the final cooled temperature.

The CO_2 absorbs heat from molten salt in the supercritical heater in the power sub-cycle, which indicates that the mass flow rate in the power sub-cycle is relative to the outlet temperature of the molten salt and the inlet temperature of CO_2 in the supercritical heater. Even though the heat capacity of molten salt decreases because of the increase of the outlet temperature of the molten salt, the mass flow rate in the power sub-cycle still increases with cooled pressure because the specific enthalpy rise of CO_2 in the supercritical heater strongly decreases. As shown in Fig. 4, the proportion increases rapidly when the cooled pressure is lower than 10 MPa and increases slowly in other conditions with raising the cooled pressure. From this perspective, it is also confirmed that the near-critical conditions are a little difficult to control. For example, the increase of the ambient temperature and the cooling water temperature may lead to an increase of the CO_2 flow rate in the refrigeration sub-cycle that is only an auxiliary cycle and a decrease of the whole cycle performance. In that case, more cooling water and a higher cooled pressure are needed to stabilize the operating condition. Under the optimal cooled pressure, the proportion of saturated liquid to total fluid is 0.85.

As shown in Fig. 5a, there is a minimum value and a maximum value for nearly all the curves, except the one with a final cooled temperature of 31 °C. The exceptional curve only shows a peak without a minimum. When the cooled pressure is lower than 11.0 MPa, the outlet temperature of the cooling water is negatively correlated with the final cooled temperature while there is almost no difference between these two parameters in the other conditions. The pinch point position plays a major role in determining the outlet temperature of the cooling water. A complex shift of the pinch point position leads to the minimum on each curve.

The heat transfer process affects the variation of the working fluid states. Therefore, this process is usually shown in the temperature-entropy diagram, which connects it with the working fluid state points of the thermodynamic cycle. As shown in Fig. 5b, values of the horizontal and vertical axis represent the relative position of the pinch point according to the state points of CO_2 in the cooler. When the cooled pressure is low, the entropy of the pinch point declines firstly and then increases with raising the cooled pressure. In other words, the pinch point shifts to the left firstly and shifts right secondly in the temperature-entropy diagram. The movement towards the left is helpful for reducing the outlet temperature of the cooling water while the shift to the right leads to an increase of that temperature. That phenomenon is the reason for the local minimum of each curve. When the cooled pressure is high, the pinch point shifts towards the left only and its temperature shows a maximum with still raising the cooled pressure. The movement of the pinch point is helpful for raising the outlet temperature of the cooling water while the maximum of the pinch point temperature causes the peak on the curve of the outlet temperature of cooling water. Under a cooled pressure of 8.0 MPa, the pinch point appears nearly at the same position (the entrance of cooler) for final cooled temperatures of 39 °C and 40 °C, respectively. As a result, the outlet temperature of the cooling water is almost the same in these two conditions. It is worth noting that the curve of the pinch point position is a little not smooth with a final cooled temperature of 40 °C and a cooled pressure from 8.0 to 8.5 MPa, as shown in Fig. 5b. The reason may be that the computation points are not dense enough. The curve may become smooth by adding some computation points in the considered range. Under the optimal cooled pressure, the outlet temperature of the cooling water is 57.3 °C with a pinch point temperature in the cooler of 59.1 °C.

As shown in Fig. 6, the net output power decreases with increasing the final cooled temperature and shows a peak with raising the cooled pressure. In the optimal conditions, the net output power is 1689.70 kW. It is determined by the turbine's power output, the pump's power consumption, the expander's power output and the compressor's power consumption, as shown in Eq. (6). The power output of the turbine plays a major role in determining the trend of the net output power curve and in the optimal condition, the turbine outputs 2473.13 kW of a power that is much higher than the pump's power consumption, the expander's power output and the compressor's power consumption. The net output power is the product of the heat capacity in the supercritical heater and the thermal efficiency. The turbine outlet temperature increases with raising the cooled pressure, which causes an increase of the inlet temperature of the CO_2 at the entrance of the heater. Then the outlet temperature of the molten salt increases while

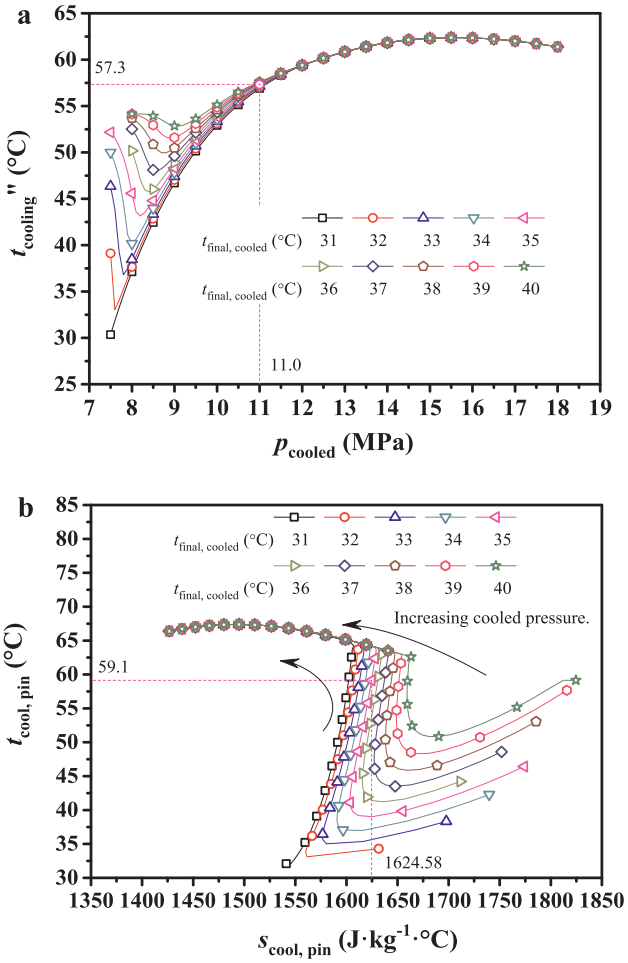

Fig. 5. Outlet temperatures of cooling water and the pinch point position in the cooler. (a Outlet temperature of cooling water; b Pinch point position in cooler).

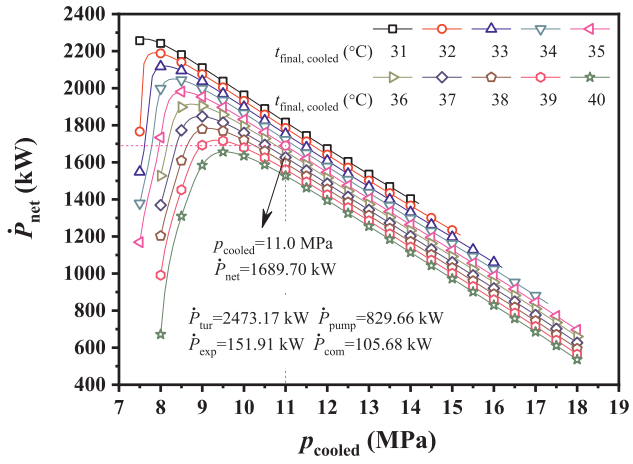

Fig. 6. Variation of the net output power with cooled pressure under different final cooled temperatures.

the heat capacity in the heater decreases correspondingly with the increase of the cooled pressure. In the other hand, the thermal efficiency increases monotonically or shows a peak with raising the cooled pressure. Therefore, a peak appears on the net output power curve in almost all the conditions.

3.2. Optimization of the condensing temperature

In the above analysis, an optimal condition is obtained with a constant condensing temperature of 20 °C. Thermal efficiency can reach up to 0.2420 with a cooled pressure of 11.0 MPa. In this section, the effect of the condensing temperature on the thermal efficiency is analysed. The condensing temperature varies from 16 °C to 30 °C, while other parameters are specified the same as the above section.

As shown in Fig. 7, the optimal thermal efficiency and the corresponding cooled pressure are obtained at each condensing temperature. The optimal thermal efficiency increases with increasing the condensing temperature and finally reaches a maximum value of 0.3463. The above optimal condition with the condensing temperature of 20 °C is also on the thermal efficiency curve. In other words, each point on the thermal efficiency curve corresponds to an optimal condition with a constant condensing temperature and an optimal cooled pressure which is indicated on the cooled pressure curve. The optimal cooled pressure curve increases firstly and then decreases with raising the condensing temperature. When the condensing temperature is 30.0 °C, the optimal thermal efficiency reaches a maximum with an optimal cooled pressure of 8.60 MPa. However, though the thermal efficiency increases monotonically with raising the condensing temperature, it is suggested to specify a relative low condensing temperature, e. g. 25 °C, to avoid a near-critical compression. There is another interesting phenomenon observed. There seems to be an inflection point for the optimal thermal efficiency curve with a final cooled temperature of approximately 21.8 °C. When the final cooled temperature is lower than 21.8 °C, the optimal cooled pressure increases and accelerates with raising the condensing temperature. Nevertheless, when the final cooled temperature is higher than 21.8 °C, the optimal cooled pressure decreases and tends to a constant with raising the condensing temperature.

It is generally known that the supercritical CO_2 Brayton cycle is widely studied and has many advantages, such as a high thermal efficiency, a compact system and an environmentally friendly working fluid. Therefore, an optimal thermal efficiency of the supercritical CO_2 Brayton cycle is also shown in Fig. 7. When the final cooled temperature is 35 °C and optimal cooled pressure is 8.1 MPa, the thermal efficiency of the supercritical CO_2 Brayton cycle reaches 0.3776. The maximum thermal efficiency of the supercritical CO_2 Brayton cycle is a little higher than that of the self-condensing CO_2 transcritical cycle by 0.0313. The decrease of the thermal efficiency is the cost paid for a liquid compression.

The compressor for the supercritical CO_2 Brayton cycle is a key component and it is difficult to develop an efficient one. Additionally, it usually operates in near critical region where the liquid hammer is very harmful to the impeller. However, a pump is used to pressurize CO_2 in liquid state for the self-condensing CO_2 transcritical cycle which simplifies the development of the pressurizing component and avoids the liquid hammer in the pressurizing process. In addition, a liquid pressurizing method can also reduce the power consumption. There are even pump products for pressurizing liquid CO_2 to a very high pressure which is sufficiently high for a CO_2 power cycle. Therefore, it is worthwhile to investigate the self-condensing CO_2 transcritical cycle and its potential for a practical application.

4. Conclusions

With solar thermal energy as a heat source, the self-condensing CO_2 transcritical cycle is optimized with a theoretical approach. Some important conclusions regarding the relationships among the cycle parameters and the optimization results of this cycle are as follows.

(1) With a low final cooled temperature, the thermal efficiency increases with raising the cooled pressure. The curve shows a peak with a final cooled temperature higher than 32 °C. At 35 °C of the final cooled temperature, the maximum thermal efficiency is 0.2420 with an optimal cooled pressure of 11.0 MPa.
(2) The proportion of the saturated liquid to the total fluid in the separator varies extremely rapidly under low cooled pressure. The complicated variation of the outlet temperature of the cooling water is mainly determined by the shift of the pinch point position in the cooler. Under 11.0 MPa of the cooled pressure, the proportion of the saturated liquid to the total fluid is 0.85 and the outlet temperature of the cooling water is 57.3 °C.
(3) In the considered conditions, the maximum thermal efficiency of the self-condensing CO_2 transcritical cycle is 0.3463, which is 0.0313 lower than that of the supercritical CO_2 Brayton cycle. However, the former cycle uses a pump to pressurize CO_2 in a liquid state, simplifies the development of pressurizing component and avoids the liquid hammer in pressurizing process.

Acknowledgements

Project 51776215 supported by National Natural Science Foundation of China is gratefully acknowledged. This study was also supported by Beijing Natural Science Foundation (3192042, 3172008).

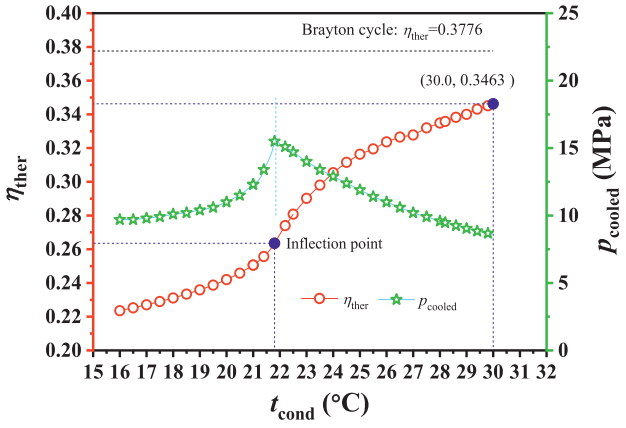

Fig. 7. Variation of the thermal efficiency and the optimal cooled pressure with condensing temperature.

References

[1] Pan L, Wang H. Improved analysis of Organic Rankine Cycle based on radial flow turbine. Appl Therm Eng 2013;61(2):606–15.
[2] Ge YT, Li L, Luo X, Tassou SA. Performance evaluation of a low-grade power generation system with CO_2 transcritical power cycles. Appl Energy 2018;227:220–30.
[3] Wang K, Li M, Guo J, Li P, Liu Z. A systematic comparison of different S-CO_2 Brayton cycle layouts based on multi-objective optimization for applications in solar power tower plants. Appl Energy 2018;212:109–21.
[4] Chen Y, Pridasawas W, Lundqvist P. Dynamic simulation of a solar-driven carbon dioxide transcritical power system for small scale combined heat and power production. Sol Energy 2010;84(7):1103–10.
[5] Ding T, Liang L, Li Z. Analytics of rankine cycle system using CO_2 as working fluid. J Eng Thermophys 2015;36(2):410–3.
[6] Zhang X, Yamaguchi H, Uneno D. Experimental study on the performance of solar Rankine system using supercritical CO_2. Renew Energy 2007;32(15):2617–28.
[7] Zhang X, Yamaguchi H, Cao Y. Hydrogen production from solar energy powered supercritical cycle using carbon dioxide. Int J Hydrogen Energ 2010;35(10):4925–32.
[8] Pan L, Wei X, Li B, Li T. Experimental investigation on the CO_2 transcritical power cycle. Energy 2016;95:247–54.
[9] Shi L, Shu G, Tian H, Huang G, Chen T, Li X, et al. Experimental comparison between four CO_2-based transcritical Rankine cycle (CTRC) systems for engine waste heat recovery. Energ Convers Manage 2017;150(15):159–71.
[10] Kim YM, Kim CG, Favrat D. Transcritical or supercritical CO_2 cycles using both low and high-temperature heat sources. Energy 2012;43(1):402–15.
[11] Wang K, He Y, Zhu H. Integration between supercritical CO_2 Brayton cycles and molten salt solar power towers: A review and a comprehensive comparison of different cycle layouts. Appl Energy 2017;195:819–36.
[12] Minh TL, Dia M, Robbie M, Ali A. Dynamic modelling and start-up operation of a solar-assisted recompression supercritical CO_2 Brayton power cycle. Appl Energy 2017;199:247–63.
[13] Chacartegui R, Alovisio A, Ortiz C, Valverde JM, Verda V, Becerra JA. Thermochemical energy storage of concentrated solar power by integration of the calcium looping process and a CO_2 power cycle. Appl Energy 2016;173:589–605.
[14] Xu C, Zhang Q, Yang Z, Li X, Xu G, Yang Y. An improved supercritical coal-fired power generation system incorporating a supplementary supercritical CO_2 cycle. Appl Energy 2018;231:1319–29.
[15] Olumayegun O, Wang M, Oko E. Thermodynamic performance evaluation of supercritical CO_2 closed Brayton cycles for coal-fired power generation with solvent-based CO_2 capture. Energy 2019;166:1074–88.
[16] Moullec YL. Conceptual study of a high efficiency coal-fired power plant with CO_2 capture using a supercritical CO_2 Brayton cycle. Energy 2013;49:23–46.
[17] Sun Z, Wang J, Dai Y, Wang J. Exergy analysis and optimization of a hydrogen production process by a solar-liquefied natural gas hybrid driven transcritical CO_2 power cycle. Int J Hydrogen Energ 2012;37:18731–9.
[18] Padilla RV, Too YCS, Benito R, Stein W. Exergetic analysis of supercritical CO_2 Brayton cycles integrated with solar central receivers. Appl Energy 2016;148:348–65.
[19] Zhao P, Wang J, Dai Y, Gao L. Thermodynamic analysis of a hybrid energy system based on CAES system and CO_2 transcritical power cycle with LNG cold energy utilization. Appl Therm Eng 2015;91:718–30.
[20] Padilla RV, Too YCS, Benito R, McNaughton R, Stein W. Thermodynamic feasibility of alternative supercritical CO_2 Brayton cycles integrated with an ejector. Appl Energy 2016;169:49–62.
[21] Syblik J, Vesely L, Entler S, Stepanek J, Dostal V. Analysis of supercritical CO_2 Brayton power cycles in nuclear and fusion energy. Fusion Eng. Des. 2019. https://doi.org/10.1016/j.fusengdes.2019.02.119.
[22] Pan L, Wei X, Shi W. Performance analysis of a zeotropic mixture (R290/CO_2) for trans-critical power cycle. Chinese J Chem Eng 2015;23(3):572–7.
[23] Ge Z, Li J, Liu Q, Duan Y, Yang Z. Thermodynamic analysis of dual-loop organic Rankine cycle using zeotropic mixtures for internal combustion engine waste heat recovery. Energ Convers Manage 2018;166(15):201–14.
[24] Xia J, Wang J, Zhang G, Lou J, Zhao P, Dai Y. Thermo-economic analysis and comparative study of transcritical power cycles using CO_2-based mixtures as working fluids. Appl Therm Eng 2018;144:31–44.
[25] Dai X, Shi L, An Q, Qian W. Screening of hydrocarbons as supercritical ORCs working fluids by thermal stability. Energ Convers Manage 2016;126:632–7.
[26] Dai X, Shi L, An Q, Qian W. Thermal stability of some hydrofluorocarbons as supercritical ORCs working fluids. Appl Therm Eng 2018;128:1095–101.
[27] Pan L, Ma Y, Li T, Li H, Li B, Wei X. Investigation on the cycle performance and the combustion characteristic of two CO_2-based binary mixtures for the transcritical power cycle. Energy 2019;179:454–63.
[28] Pan L, Wei X, Shi W. Theoretical investigation on a novel CO_2 transcritical power cycle. J Eng Thermophys 2015;36(6):1182–5.
[29] Lemmon EW, Huber ML, McLinden MO. NIST Standard Reference Database 23, Reference Fluid Thermodynamic and Transport Properties (REFPROP), version 9.0. National Institute of Standards and Technology; 2010.
[30] Liao M, Wei X, Ding J, Hu B, Peng Q. Preparation and experimental investigation for LNK carbonate molten salts. Acta Energy Sin 2010;31(7):863–7.